Received: 10 August 2021 | Revised: 28 December 2021 | Accepted: 10 February 2022

DOI: 10.1002/rob.22067

RESEARCH ARTICLE

WILEY

TetraFLEX: Design and kinematic analysis of a novel self-aligning family of 3T1R parallel manipulators

Henrique Simas[1] | **Raffaele Di Gregorio**[2] | **Roberto Simoni**[3]

[1]Department of Mechanical Engineering, Federal University of Santa Catarina, Florianópolis, Santa Catarina, Brazil

[2]Department of Engineering, University of Ferrara, Ferrara, Italy

[3]Department of Mobility Engineering, Federal University of Santa Catarina, Joinville, Santa Catarina, Brazil

Correspondence

Roberto Simoni, Department of Mobility Engineering, Federal University of Santa Catarina, Joinville, Santa Catarina, Brazil.
Email: roberto.simoni@ufsc.br

Funding information

Conselho Nacional de Desenvolvimento Científico e Tecnológico; Università degli Studi di Ferrara; Coordenação de Aperfeiçoamento de Pessoal de Nível Superior

Abstract

A new family of 3T1R parallel manipulators (PMs) with self-aligning property, named TetraFLEX, is presented. 3T1R manipulators have many applications in different fields. Moreover, self-aligning property refers to the presence of passive joints in the PM limbs that are conceived to compensate for possible misalignments between the sliding directions of the actuated prismatic(P)-pairs. This property allows the fixation of the limbs in different frame geometries. Thus, this advantage broadens the PM applications to field robotics in several scenarios. Here, the position and singularity analyses of the new family of self-aligning PMs is addressed with a unified approach. The results are that both the direct and the inverse position analyses have simple closed-form solutions and that wide free-from-singularity regions of TetraFLEX PMs' workspace exist. The effectiveness of the technical proposal is also illustrated by discussing their design criteria and kinetostatics performances in a case study.

KEYWORDS

4-DOF PMs, kinematic analysis, motion simulation, Schoenflies motion, self-aligning, singularities, TetraFLEX

1 | INTRODUCTION

Many manipulation tasks and in situ operations (e.g., pick-and-place tasks of a crane, 3D printing of civil-building elements, etc.) usually require spatial translations combined with rotations around axes with one given direction. This type of motion, named Schoenflies motion, constitutes a four-dimensional (4D) sub-group of the displacement group (Hervé, 1994, 1999) and the kinematic chains that generate it are named Schoenflies-motion generators (SMGs) (Lee & Hervé, 2009b). SMGs can be used on their own or combined with other types of kinematic chains (Lee & Hervé, 2009a) to conceive architectures for manipulators with 4-degrees-of-freedom (DOF), usually named 3T1R manipulators, that perform Schoenflies motion.

In Lee and Hervé (2009b), Lee and Hervé enumerated all the serial SMGs containing only lower pairs and/or parallelograms (π joints) and gave them the name of "primitive SMGs." The most known serial SMG is of RRRP type since it was used in the first 3T1R manipulator, the SCARA robot (Makino, 1982).

Parallel manipulators (PMs) have been also proposed as 3T1R manipulators. PMs feature the end effector (platform) connected to the frame (base) through a number of kinematic chains (limbs). A simple way of obtaining 3T1R PMs is the addition of a fourth limb, for instance, of type R UPUR, which works as a transmission shaft to make the gripper rotate, to a translational PM (Carricato, 2005; Clavel, 1990; Lee & Hervé, 2009c). An additional rotational DOF can also be added to a translational PM by introducing an articulated platform together with a fourth limb similar to the other limbs (Krut et al., 2003, 2004; Pierrot & Company, 1999; Pierrot et al., 2006). Hereafter, PMs' limb topology is indicated through the string of capital letters associated to the joint types encountered by moving from the base to the platform. In such strings the

underlined letters denote the actuated joints. Also, PMs' topology is denoted as $n_1String_1 - n_2String_2 - \ldots - n_gString_g$ where n_k, for $k = 1, \ldots, g$, indicates the number of limbs of type $String_k$ that are present in the PM.

Nevertheless, 3T1R PMs can also be obtained through ad hoc architectures. In the literature, somehow exhaustive enumerations of these architectures have been presented (see, for instance, Amine et al., 2013; Carricato, 2005; Kong & Gosselin, 2004; Lee & Hervé, 2011). Listing possible architectures for 3T1R PMs does not provide many pieces of information on their characteristics and specific kinematic and dynamic analyses are necessary to highlight their qualities and defects. Therefore, many papers were published which address the analyses of particular 3T1R PMs or of 3T1R PM's classes (see, for instance, Arian et al., 2020; Gallardo-Alvarado et al., 2017; Lee & Lee, 2012, 2016; Tu et al., 2018) and the research on 3T1R PM is still alive. A simplified architecture, the possibility of putting on the base the motors that drive the actuated joints, and wide free-from-singularity workspace regions are the main sought-after features that bring to have a 3T1R PM with good performances.

In this context, these authors analyzed single-loop 3T1R architectures with actuators on the base (Di Gregorio, 2017, 2018; Simas & Di Gregorio, 2019). Also, some of the authors introduced the concept of self-aligning property with reference to a family of translational PMs, named TriFLEX (Maletz et al., 2019; Simas et al., 2017; Simoni et al., 2014, 2015). Self-aligning property refers to the presence of passive joints in the limbs that do not affect the platform motion and work only to compensate the possible presence of a misalignment between the sliding directions of the actuated P-pairs located on the base. Such a property makes the fixation of the limbs to the base easier and has potential application in several scenarios related to field robotics.

This paper presents a family of 3T1R PMs, named TetraFLEX, with self-aligning property that have four limbs with only one actuated P-pair per limb, which is located on the base. The actuated P-pairs on the base together with the self-aligning property warranty that TetraFLEX PMs can be mounted on site by using rails that do not need special manufacturing care as it is usual in field robotics.

Here, the position and the singularity analyses of TetraFLEX PMs are addressed with a unified approach. These analyses will show that both the direct and the inverse position analyses have simple closed-form solutions and that wide free-from-singularity regions of TetraFLEX PMs' workspace exist.

The paper is organized as follows. Section 2 describes the TetraFLEX family and the used notation. Sections 3 and 4 address the position and the singularity analyses, respectively. Then, Section 5 illustrates design criteria adoptable for TetraFLEX PMs and the simulation results for this family. Eventually, Section 6 discusses the results and Section 7 draws the conclusions.

2 | THE TETRAFLEX FAMILY

The TetraFLEX family is constituted of 3T1R PMs of type P XYZ-3P QVWU. In the PXYZ limb, X, Y, and Z stand for any type of single-DOF pairs so connected that the XYZ kinematic chain is a 3-DOF planar chain whose motion plane is perpendicular to the sliding direction of the P-pair. Thus the PXYZ limb has 4-DOF and is a serial SMG (Lee & Hervé, 2009b). In the three PQVWU limbs, Q, V, and W stand for any type of single-DOF pairs that suitably combined with a P-pair on the frame and an U-joint on the distal link give a 6-DOF serial kinematic chain that, when the P-pair is locked, constrains the center of the U-joint to lie on a plane perpendicular to the sliding direction of the P-pair without limiting the orientation of the distal link and the motion of the U-joint center on the same plane

In the above-mentioned P XYZ-3P QVWU architectures, the PXYZ limb, which is a primitive SMG (Lee & Hervé, 2009b), constrains the platform to perform only Schoenflies motions and the other three limbs of PQVWU type do not reduce further the platform mobility since their connectivity—"connectivity" of a limb is the DOF number that the platform would have if it were connected to the base only through that limb (Davidson & Hunt, 2004)–is equal to six (i.e., it is equal to the DOF number of a not-constrained rigid body). As a consequence, the PXYZ-3PQVWU mechanisms, the TetraFLEX family is based on, are 4-DOF not-overconstrained SMGs, which can control the platform motion by actuating the four P-pairs adjacent to the base whatever be the platform geometry provided that the sliding directions of the P-pairs are not parallel to a unique plane (i.e., they are self-aligning 3T1R PMs).

Two examples of TetraFLEX PMs are the P RRR-3P RRS of Figure 1a, where, in each limb, the R-pairs' rotation axes are all parallel to the sliding direction of the actuated P-pair, and the P RRR-3P RCU of Figure 1b, where, in each limb, the R-pairs' rotation axes are all parallel to the sliding direction of the actuated P-pair and, in the three P RCU limbs, the C-pair axis passes through the center of the U-joint and is perpendicular to the R-pair axis.

With reference to Figure 1, A_i, for $i = 2, 3, 4$, are the centers of the U-joints and A_1 is a platform point that lies on the axis of the Z joint. These four platform points uniquely define the platform geometry. The four lines, $(O_j, \mathbf{n}_j)$, with the directions of the unit vectors $\mathbf{n}_j$ and passing through the base points O_j, for $j = 1, \ldots, 4$, are fixed in the base and are parallel to the sliding directions of the four actuated P-pairs. These four lines uniquely define the base geometry. Also, a Cartesian reference $O_1 - x_1 y_1 z_1$ $(A_1 x_p y_p z_p)$, fixed to the base (the platform), with the z_1 (z_p) coordinate axis parallel to $\mathbf{n}_1$ is introduced.

It is worth noting that, since the XYZ chain is a planar kinematic chain with motion plane perpendicular to $\mathbf{n}_1$, the direction of $\mathbf{n}_1$ is fixed with respect to the platform, too. As a consequence, the $x_1 y_1$-coordinate plane of the base reference is always parallel to the $x_p y_p$-coordinate plane of the platform reference and the orientation of $A_1 x_p y_p z_p$ with respect to $O_1 - x_1 y_1 z_1$ is uniquely determined by the angle γ between the axes x_1 and x_p (see Figure 1). Thus, the platform pose is uniquely determined by the angle γ and the coordinates $(A_{1x}, A_{1y}, A_{1z})^T$ of point A_1 measured in the base reference $O_1 - x_1 y_1 z_1$, and the rotation matrix ${}^1\mathbf{R}_p$ that transforms the components of a vector measured in $A_1 x_p y_p z_p$ into the components of the same vector measured in $O_1 - x_1 y_1 z_1$ is

$$ {}^1\mathbf{R}_p = \begin{bmatrix} c_\gamma & -s_\gamma & 0 \\ s_\gamma & c_\gamma & 0 \\ 0 & 0 & 1 \end{bmatrix}, \tag{1} $$

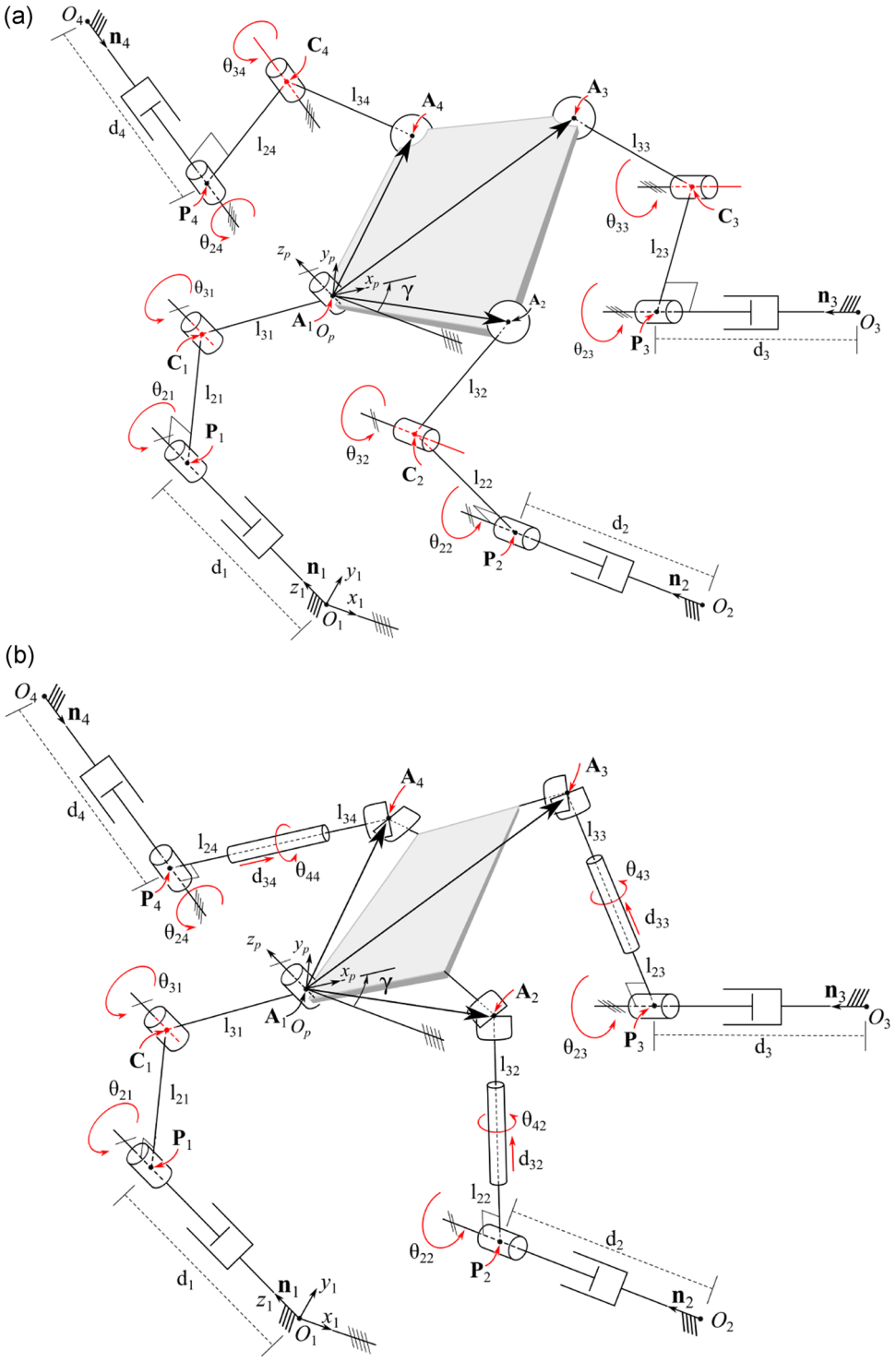

FIGURE 1 Two examples of TetraFLEX PMs: (a) P RRR-3P RRS architecture and (b) P RRR-3P RCU architecture

where s_γ and c_γ stand for $\sin\gamma$ and $\cos\gamma$, respectively. Eventually, since each limb constrains the corresponding platform-attachment-point, A_j, for $j = 1, \ldots, 4$, to lie on a plane perpendicular to the sliding direction of the actuated pair of the same limb (i.e., perpendicular to $\mathbf{n}_j$), the actuated-joint variables can be chosen equal to the distances, d_j, for $j = 1, \ldots, 4$, of the base points, O_j, for $j = 1, \ldots, 4$, from these motion planes (see Figure 1). In Figure 1, the points P_j, for $j = 1, \ldots, 4$, are the feet of the perpendiculars to such motion planes from the corresponding base points O_j. From a geometric point of view, the j-th actuated-joint variable, d_j, is equal to the length of the segment $\overline{O_jP_j}$.

The introduced notations/definitions are common to all the members of the TetraFLEX family no matter which type of pairs the

X, Y, Z, Q, V, and W are. So, all the kinematic relationships deduced by using only these notations/definitions hold for any 3T1R PM belonging to this family. In the next two sections, the position and the singularity analyses of TetraFLEX PMs will be addressed by using only these notations/definitions thus providing general results that hold for any member of the TetraFLEX family.

3 | POSITION ANALYSIS

Position analysis consists in the solution of two problems: the *Forward position analysis* (FPA), and the *Inverse position analysis* (IPA). The FPA is the determination of all the platform poses compatible with assigned values of the actuated-joint variables. Vice versa, the IPA, is the determination of actuated-joint variables' values compatible with an assigned platform pose.

3.1 | Forward position analysis

In the case of a TetraFLEX PM, the platform pose is uniquely identified by the 4-tuple $\mathbf{p} = (A_{1x}, A_{1y}, A_{1z}, \gamma)^T$. As a consequence, its FPA is the determination of the $\mathbf{p}$ values compatible with an assigned value of the 4-tuple $\mathbf{q} = (d_1, d_2, d_3, d_4)^T$, which collects all the actuated-joint variables.

The fact that each platform point A_j must lie on a specific motion plane makes the equations of these four motion planes coincide with the closure equations of a TetraFLEX PM. Such equations are

$$(A_j\text{-}O_j) \cdot \mathbf{n}_j = d_j, \quad j = 1, \ldots, 4. \tag{2}$$

The replacement, into Equation (2), of the following relationships

$$\mathbf{A}_j = \mathbf{A}_1 +^1 \mathbf{R}_p^{pA_j}, \quad j = 1, \ldots, 4 \tag{3}$$

yields, after the introduction of formula (1) and the expansion of the resulting formulas, the following equation system (n_{jx}, n_{jy}, and n_{jz} are the components of $\mathbf{n}_j$ measured in $O_1 - x_1 y_1 z_1$):

$$\mathbf{A}_1 \cdot \mathbf{n}_j + \left(A_{jx}^p c_\gamma - A_{jy}^p s_\gamma\right) n_{jx} + \left(A_{jx}^p s_\gamma + A_{jy}^p c_\gamma\right) n_{jy} + A_{jz}^p n_{jz} - \mathbf{O}_j \cdot \mathbf{n}_j = d_j, j = 1, \ldots, 4 \tag{4}$$

which can be rewritten as follows:

$$A_{1z} = d_1, \tag{5a}$$

$$A_{1x} n_{jx} + A_{1y} n_{jy} + a_j c_\gamma + b_j s_\gamma = k_j \quad j = 2, 3, 4, \tag{5b}$$

with

$$a_j = A_{jx}^p n_{jx} + A_{jy}^p n_{jy} = h_j c_{\alpha_j}, \tag{6a}$$

$$b_j = A_{jx}^p n_{jy} - A_{jy}^p n_{jx} = h_j s_{\alpha_j}, \tag{6b}$$

$$k_j = \mathbf{O}_j \cdot \mathbf{n}_j + d_j - \left(A_{jz}^p + d_1\right) n_{jz} \tag{6c}$$

where h_j and α_j are geometric constants defined as follows:

$$h_j = \sqrt{\left[\left(A_{jx}^p\right)^2 + \left(A_{jy}^p\right)^2\right]\left(n_{jx}^2 + n_{jy}^2\right)}, \tag{7a}$$

$$\alpha_j = \operatorname{atan2}\left(A_{jx}^p n_{jy} - A_{jy}^p n_{jx}, A_{jx}^p n_{jx} + A_{jy}^p n_{jy}\right). \tag{7b}$$

From a geometric point of view, h_j is the product of the magnitudes of the projections of the two constant vectors ${}^p\mathbf{A}_j$ and $\mathbf{n}_j$ onto the $x_1 y_1$-coordinate plane; whereas, α_j is the angle between the projections onto the $x_1 y_1$-coordinate plane of the constant vectors ${}^p\mathbf{A}_j$ and $\mathbf{n}_j$ (see Figures 1 and 2).

In the FPA, the coefficients a_j, b_j and k_j are known constants since they depend only on geometric constants and on the values of the actuated joint variables, which are assigned. Therefore, system (5) is linear in the platform-position variables, A_{1x}, A_{1y}, and A_{1z}, and depend on depend on γ (i.e., on the platform orientation) through simple trigonometric functions. The linear elimination of the platform-position unknowns from the first three equations of system 5 yields the following explicit expressions of them

$$A_{1x} = \frac{(k_2 - a_2 c_\gamma - b_2 s_\gamma) n_{3y} - (k_3 - a_3 c_\gamma - b_3 s_\gamma) n_{2y}}{n_{2x} n_{3y} - n_{2y} n_{3x}}, \tag{8a}$$

$$A_{1y} = \frac{(k_3 - a_3 c_\gamma - b_3 s_\gamma) n_{2x} - (k_2 - a_2 c_\gamma - b_2 s_\gamma) n_{3x}}{n_{2x} n_{3y} - n_{2y} n_{3x}}, \tag{8b}$$

$$A_{1z} = d_1, \tag{8c}$$

whose introduction into the fourth equation of system (5) gives the following univariate trigonometric equation:

$$a_c c_\gamma + b_c s_\gamma = k_c, \tag{9}$$

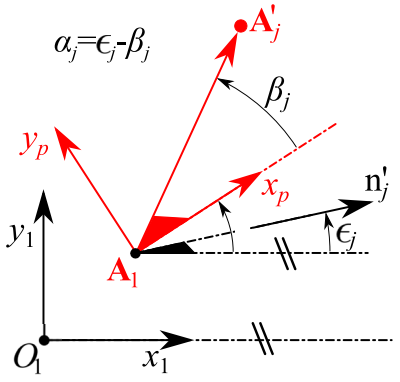

FIGURE 2 Geometric definition of the angle α_j (A'_j and $\mathbf{n}'_j$ are the projections onto the $x_1 y_1$-coordinate plane of A_j and $\mathbf{n}_j$, respectively)

where

$$a_c = a_2(n_{3x}n_{4y} - n_{3y}n_{4x}) + a_3(n_{2y}n_{4x} - n_{2x}n_{4y}) + a_4(n_{2x}n_{3y} - n_{2y}n_{3x}), \tag{10a}$$

$$b_c = b_2(n_{3x}n_{4y} - n_{3y}n_{4x}) + b_3(n_{2y}n_{4x} - n_{2x}n_{4y}) + b_4(n_{2x}n_{3y} - n_{2y}n_{3x}), \tag{10b}$$

$$k_c = k_2(n_{3x}n_{4y} - n_{3y}n_{4x}) + k_3(n_{2y}n_{4x} - n_{2x}n_{4y}) + k_4(n_{2x}n_{3y} - n_{2y}n_{3x}). \tag{10c}$$

From a geometric point of view, the coefficients $(n_{rx}n_{sy} - n_{ry}n_{sx})$ with $r, s \in \{2, 3, 4 | r \neq s\}$ that appear in Equation (10) are equal to zero when the projections onto the $x_1\,y_1$-coordinate plane of the two unit vectors $\mathbf{n}_r$ and $\mathbf{n}_s$ are parallel to one another.

The introduction of the trigonometric identities $c_\gamma = \frac{1-t^2}{1+t^2}$ and $s_\gamma = \frac{2t}{1+t^2}$, where $t = \tan\frac{\gamma}{2}$ with $\gamma \in]-\pi, \pi]$, into Equation (9), after some algebraic manipulations, transforms it into the quadratic equation:

$$(k_c + a_c)t^2 - 2b_c t + (k_c - a_c) = 0, \tag{11}$$

which gives the following two solutions for t:

$$t_n = \frac{b_c + (-1)^n\sqrt{b_c^2 + a_c^2 - k_c^2}}{k_c + a_c}, n = 1, 2. \tag{12}$$

Accordingly, the values of γ that solve Equation (11) are two:

$$\gamma_n = 2\arctan(t_n), n = 1, 2. \tag{13}$$

The back-substitution of these two values of γ into formulas (8) gives as many values for the platform-position variables (A_{1x}, A_{1y}, A_{1z}). Therefore, the conclusion is that the FPA of any TetraFLEX PM has two solutions, which can be determined through the explicit formulas (8) and (13).

3.2 | Inverse position analysis

The IPA of a TetraFLEX PM is the determination of the actuated-joint-variables' values (i.e., of $\mathbf{q} = (\mathrm{d}_1, \mathrm{d}_2, \mathrm{d}_3, \mathrm{d}_4)^T$) compatible with one assigned platform pose (i.e., for one assigned value of $\mathbf{p} = (A_{1x}, A_{1y}, A_{1z}, \gamma)^T$). Since the closure Equations (4) are explicit expressions of the actuated-joint variables as functions of the geometric constants and of the platform-pose variables, the IPA solution is unique and trivial.

4 | INSTANTANEOUS KINEMATICS ANALYSIS

The analysis of the instantaneous kinematics of a PM deals with the determination and the analysis of its instantaneous input/output relationship. The instantaneous input/output relationship in general states a one-to-one correspondence between the tuple collecting the actuated-joint rates and the platform twist or, as an alternative, the tuple collecting the first time-derivatives of the variables that uniquely determine the platform pose. It is always a linear and homogeneous system whose coefficient matrices depend only on the PM configuration. It is the system to solve for solving the two problems of PMs' instantaneous kinematics: the forward instantaneous kinematics problem (FIKP) and the inverse instantaneous kinematics problem (IIKP). The FIKP is the determination of the platform twist (or, the first time-derivatives of the variables that uniquely determine the platform pose) once the actuated-joint rates are assigned. Vice versa, The IIKP is the determination of the actuated-joint rates once the platform twist (or, the first time-derivatives of the variables that uniquely determine the platform pose) is known.

In the case of a TetraFLEX PM, the instantaneous input/output relationship must relate $\dot{\mathbf{q}} = (\dot{\mathrm{d}}_1, \dot{\mathrm{d}}_2, \dot{\mathrm{d}}_3, \dot{\mathrm{d}}_4)^T$ to $\dot{\mathbf{p}} = (\dot{A}_1 x, \dot{A}_1 y, \dot{A}_1 z, \dot{\gamma})^T$. It can be deduced by time-differentiating closure-equation system (5). In so doing, the following instantaneous input/output relationship is obtained

$$\dot{A}_{1z} = \dot{d}_1, \tag{14a}$$

$$\dot{A}_{1x}n_{jx} + \dot{A}_{1y}n_{jy} + h_j(s_{\alpha_j}c_\gamma - c_{\alpha_j}s_\gamma)\dot{\gamma} = \dot{d}_j - \dot{d}_1 n_{jz} \quad j = 2, 3, 4, \tag{14b}$$

whose matrix form is

$$\mathbf{M}\dot{\mathbf{p}} = \mathbf{N}\dot{\mathbf{q}} \tag{15}$$

with

$$\mathbf{M} = \begin{bmatrix} 0 & 0 & 1 & 0 \\ n_{2x} & n_{2y} & 0 & h_2 s_{(\alpha_2-\gamma)} \\ n_{3x} & n_{3y} & 0 & h_3 s_{(\alpha_3-\gamma)} \\ n_{4x} & n_{4y} & 0 & h_4 s_{(\alpha_4-\gamma)} \end{bmatrix}, \mathbf{N} = \begin{bmatrix} 1 & 0 & 0 & 0 \\ -n_{2z} & 1 & 0 & 0 \\ -n_{3z} & 0 & 1 & 0 \\ -n_{4z} & 0 & 0 & 1 \end{bmatrix}, \tag{16}$$

where the trigonometric identities $s_{(\alpha_j-\gamma)} = (s_{\alpha_j}c_\gamma - c_{\alpha_j}s_\gamma)$, for $j = 2, 3, 4$, have been used.

4.1 | Singularity analysis

The PM configurations where the instantaneous input/output relationship fails to state a one-to-one correspondence between platform twist and actuated-joint rates are named singularities. PM singularities are usually collected into three sets (Gosselin & Angeles, 1990): the ones that make the IIKP unsolvable (type-I singularities), the ones that make the FIKP unsolvable (type-II singularities), and those that make both the IIKP and the FIKP unsolvable (type-III singularities). From a kinematic point of view (Agrawal, 1991), the instantaneous mobility of the platform is reduced at a type-I singularity, which involves that type-I singularities occurs at the workspace boundaries; whereas, the actuators are not able to control the platform twist any longer at a type-II singularity, which, in lower-mobility PMs, may correspond to a local increase of the platform instantaneous mobility (Di Gregorio, 2020). Lower-mobility PMs

are those whose DOF number is lower than six, 3T1R PMs are lower-mobility PMs. Also, a special case of type-II singularities, named "constraint singularities," can make the platform of a lower-mobility PM change is type of motion (Zlatanov et al., 2002); they may occur only in lower-mobility PMs containing only limbs with connectivity higher than the DOF number of the PM (Di Gregorio, 2020), which is not the case of TetraFLEX PMs.

In the case of TetraFLEX PMs, system (15) states a one-to-one correspondence between $\dot{\mathbf{p}}$ and $\dot{\mathbf{q}}$ when both the 4 × 4 matrices **M** and **N** are full rank. Type-I singularities occur when **N** is rank deficient. Since **N** is a constant matrix with $\det(\mathbf{N}) = 1$ (i.e., always non-null), there are no type-I and type-III singularities in TetraFLEX PMs. Type-II singularities occur when **M** is rank deficient, that is, when its determinant is equal to zero. The analysis of matrix **M** reveals that $\det(\mathbf{M})$ can be written as follows

$$\det(\mathbf{M}) = \mathbf{e} \cdot (\mathbf{f} \times \mathbf{g}) \tag{17}$$

with

$$\mathbf{e} = \begin{pmatrix} h_2 s_{(\alpha_2-\gamma)} \\ h_3 s_{(\alpha_3-\gamma)} \\ h_4 s_{(\alpha_4-\gamma)} \end{pmatrix} = \begin{pmatrix} b_2 c_\gamma - a_2 s_\gamma \\ b_3 c_\gamma - a_3 s_\gamma \\ b_4 c_\gamma - a_4 s_\gamma \end{pmatrix}, \mathbf{f} = \begin{pmatrix} n_{2x} \\ n_{3x} \\ n_{4x} \end{pmatrix}, \mathbf{g} = \begin{pmatrix} n_{2y} \\ n_{3y} \\ n_{4y} \end{pmatrix}. \tag{18}$$

From a geometric point of view, the analysis of Equation (17) reveals that

i. $\det(\mathbf{M})$ and, as a consequence, possible type-II singularities depend only on the projection on the $x_1 y_1$-coordinate plane of geometric constants of the PM;
ii. $\det(\mathbf{M})$ depends only on γ (i.e., on the orientation of the platform);
iii. the vectors **f** and **g** are constant; as a consequence, an architecture singularity (i.e., a special sizing of the PM that makes all the PM configurations singular) Ma and Angeles (1991) occurs when **f** and **g** are parallel to one another;
iv. an architecture singularity also occurs if $n_{jx} = n_{jy} = 0$ for a j value not equal to 1. Indeed, in this case, also $a_j = b_j = 0$ and, as a consequence, **M** has a null row (i.e., is singular);
v. out of architecture singularities, a type-II singularity occurs when the three vectors **e**, **f**, and **g** are coplanar.

From an analytic point of view, by expanding (17) and equating to zero the resulting expression, the following singularity equation comes out:

$$\det(\mathbf{M}) = b_c c_\gamma - a_c s_\gamma = 0, \tag{19}$$

where b_c and a_c are the constants defined by the formulas (10).

Equation (19) can be rearranged as follows:

$$\tan(\gamma) = \frac{b_c}{a_c}. \tag{20}$$

Equation (20) reveals that, by excluding architecture singularities, there are always (i.e., whatever be the sizing of the PM) only two type-II singularities, which are identified by two γ values separated by π rad.

Such values can be numerically computed by introducing the trigonometric identities $c_\gamma = \frac{1-t^2}{1+t^2}$ and $s_\gamma = \frac{2t}{1+t^2}$, where $t = \tan\frac{\gamma}{2}$ with $\gamma \in \,]-\pi, \pi]$, into Equation (19), to transform it into the quadratic equation:

$$b_c t^2 + 2a_c t - b_c = 0, \tag{21}$$

which gives the following two solutions for t:

$$t_n = \frac{-a_c + (-1)^n \sqrt{a_c^2 + b_c^2}}{b_c}, \quad n = 1, 2. \tag{22}$$

Accordingly, the values of γ that solve Equation (19) are $\gamma_n = 2\arctan(t_n)$ for $n = 1, 2$.

5 | DESIGN CRITERIA

The above-reported singularity analysis highlights that architecture singularities can be avoided by choosing the unit vectors $\mathbf{n}_j$, for $j = 2, 3, 4$, so that none of them is parallel to the z_1-coordinate axis (see condition (iv)), and their projections onto the $x_1 y_1$-plane are not all parallel (see condition (iii)).

Also, Equations (15) and (16) reveal that, by choosing all the unit vectors $\mathbf{n}_j$, for $j = 2, 3, 4$, parallel to the $x_1 y_1$-plane, matrix **N** becomes an identity matrix which simplify the kinematics model.

Eventually, the position of the two type-II singularities identified by Equation (20) can be located where the designer wants by suitably choosing the values of the angles α_j for $j = 2, 3, 4$. More than that, singularities can be eliminated from the useful workspace by sizing the geometry of the platform and the base of TetraFLEX.

The above-identified criteria are used in the definition of the TetraFLEX PM's nominal geometry in following section.

5.1 | Case study

This section presents a case study to exemplify the applicability of TetraFLEX in unstructured environments of field robotics. Without loosing generality, the PRRR + 3PRRS TetraFLEX was selected to conduct the case study. The objective is to improve the kinematic performance as functions of the platform geometry and the directions of the actuated joints. Beyond that, it will be demonstrated that inaccuracies in the installation of the base do not compromise the performance of the robot and singularities can be avoided by correctly choosing the range of γ.

The TetraFLEX platform is geometrically constituted by four points A_j, $j = 1, 2, 3, 4$ with fixed coordinates measured in the reference $O_p - x_p y_p z_p$, making part of the relations that define the differential kinematics (see Figure 1 and Equations 2 and 3). In this sense, the platform geometry and the $\mathbf{n}_j$ vectors, allow us to calculate and keep TetraFLEX away from singular postures, as discussed in

Section 4. An adequate measure of singularity distance is the Conditioning Index (CI) because it measure the amplification of the errors between inputs and outputs in kinematic and static models (Gosselin & Angeles, 1991; Merlet, 2006). According to Gosselin and Angeles (1991), CI is defined as the inverse of the condition number, k, of the Jacobian. In the studied case, using the Euclidean norm of the Jacobian, the condition number of a manipulator is defined by

$$k = \|\mathbf{M}\| \, \|\mathbf{M}^{-1}\|, \tag{23}$$

which measure the ratio of the largest to the smallest singular value of $\mathbf{M}^{-1}$ Simas and Di Gregorio (2017).

Higher values for CI = $1/k$ imply better kinematic performances in terms of accuracy and distance from singularity. The highest value for CI is 1, which means that the robot is in an optimal configuration called isotropic (Gosselin & Angeles, 1991).

To apply CI as a performance index to TetraFLEX, the problem of homogenization present in Equation (15) must be solved. This can be done by choosing a characteristic length, l, of the platform to define $h_j^* = h_j/l$, for $j = 2, 3, 4$, and $\gamma^* = l\gamma$, which are used for changing the output tuple from $\mathbf{p}$ to $\mathbf{p}^* = [A_1, \gamma^*]$ and the Jacobian from $\mathbf{M}$ to the dimensionless Jacobian $\mathbf{M}^*$ defined as follows:

$$\mathbf{M}^* = \begin{bmatrix} 0 & 0 & 1 & 0 \\ n_{2x} & n_{2y} & 0 & h_2^* s_{(\alpha_2-\gamma)} \\ n_{3x} & n_{3y} & 0 & h_3^* s_{(\alpha_3-\gamma)} \\ n_{4x} & n_{4y} & 0 & h_4^* s_{(\alpha_4-\gamma)} \end{bmatrix}. \tag{24}$$

Hereafter, the choice l = 1 l.u.—*length unit*—is adopted since it corresponds to the distance between ${}^p\mathbf{A}_1$ and ${}^p\mathbf{G}_b$, which is a reference size of the platform, as shown in the geometric scheme of Figure 3.

This case study makes a numerical search of the geometrical variables of the platform and $\mathbf{n}_j$ vectors, to control and limit distances from singularities, using the CI as a parameter to be optimized.

Consider the geometric scheme for the platform shown in Figure 3 in which ${}^p\mathbf{A}_1 = (0, 0, 0)^T$, ${}^p\mathbf{G}_a = (1, 0, 0)^T$, ${}^p\mathbf{G}_b = (0, 1, 0)^T$. Also, let r_1 and r_2 be two support lines. Line r_1, defined by the points

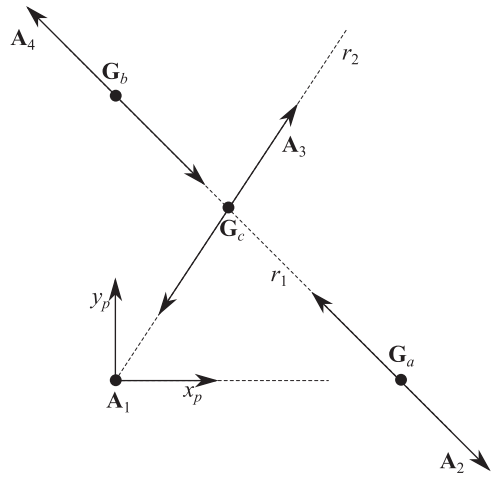

FIGURE 3 Geometry scheme of the platform for CI' optimization

${}^p\mathbf{G}_a$ and ${}^p\mathbf{G}_b$, will serve as reference to set the points ${}^p\mathbf{A}_2$, ${}^p\mathbf{A}_4$, and the point ${}^p\mathbf{G}_c$ calculated by the linear parameter u as follows.

$${}^p\mathbf{G}_c = (1 - u) \; {}^p\mathbf{G}_a + (u){}^p\mathbf{G}_b. \tag{25}$$

Line r_2 defined by the points ${}^p\mathbf{A}_1$ and ${}^p\mathbf{G}_c$, will serve as reference to the coordinates of ${}^p\mathbf{A}_3$ (see Figure 3).

The coordinates of ${}^p\mathbf{A}_2$, ${}^p\mathbf{A}_3$ and ${}^p\mathbf{A}_4$ are given by

$${}^p\mathbf{A}_2 = (1 - v) \; {}^p\mathbf{G}_a + (v) \; {}^p\mathbf{G}_b, \tag{26}$$

$${}^p\mathbf{A}_3 = (1 - w) \; {}^p\mathbf{A}_1 + (w) \; {}^p\mathbf{G}_c, \tag{27}$$

$${}^p\mathbf{A}_4 = (1 - v) \; {}^p\mathbf{G}_b + (v) \; {}^p\mathbf{G}_a, \tag{28}$$

where v and w together with u are real parameters that make the platform geometry change during optimization.

A triangular geometry of the platform is obtained fixing u = 0.5 and w = 1 and computing ${}^p\mathbf{A}_2$ and ${}^p\mathbf{A}_4$ by changing the parameter v. A quadrilateral geometry is obtained by computing the coordinates of ${}^p\mathbf{A}_3$ changing the values of u (Equation 25) and w. Triangular and quadrilateral geometries are a common proposition for platforms of PMs in several works (Briot & Bonev, 2009; Briot & Bonev, 2010; Gosselin, 2009; Gosselin et al., 2007; Pierrot et al., 2009; Rat et al., 2010; Simas & Di Gregorio, 2019; Simoni et al., 2014, 2015; Simas et al., 2017).

According to the above definitions, $\mathbf{n}_1 = (0, 0, 1)$ is the unity vector of z_1-axis (see Equation 3). In this optimization, $\mathbf{n}_2$ is fixed and equal to $(1, 0, 0)$. The remain part of the geometry is defined as functions of the following six variables: ϵ_3, ϵ_4, γ, u, v and w. The search ranges of these variables are chosen as follows:

- $u, v, w \in [-2; 2]$,
- $\epsilon_3, \epsilon_4 \in [0; \pi]$,
- $\gamma \in [-\pi/2; \pi/2]$.

These values have been chosen after a trial-and-error procedure.

An initial analysis searches for the maximum value of CI in the case of a triangular platform with w = 1.0 and u = 0.5. Figure 4 shows the results, with the reference to Figure 4 the maximum CI value is 0.809, for v = −0.35, ϵ_3 = 2.1 rad, ϵ_4 = 1.05 rad, γ = −0.2708 rad. The search algorithm based on nested loops ran in a Notebook Intel-Core i3 2.20 GHz, with 20 Gb RAM, in the processing time of 147 s.

Figure 5 shows the top view of the 3D diagram of Figure 4 with the contour curves. In Figure 5, the region highlighted in yellow keeps CI>0.6 which provides TetraFLEX manipulators with acceptable kinematic performances (Gosselin & Angeles, 1991).

Now changing u and w in the range $[-2, 2]$, the platform can assume quadrilateral shape. Again, another search algorithm based on nested loop was applied to study the individual influence of u and w on CI.

Figure 6 presents the CI as a function of u and γ.

It is worth noting that (see Figure 6) the maximum CI does not change for the same γ with respect to the parameter u, but the edges of the surface assume higher values for CI for u = 0.5. Thus the

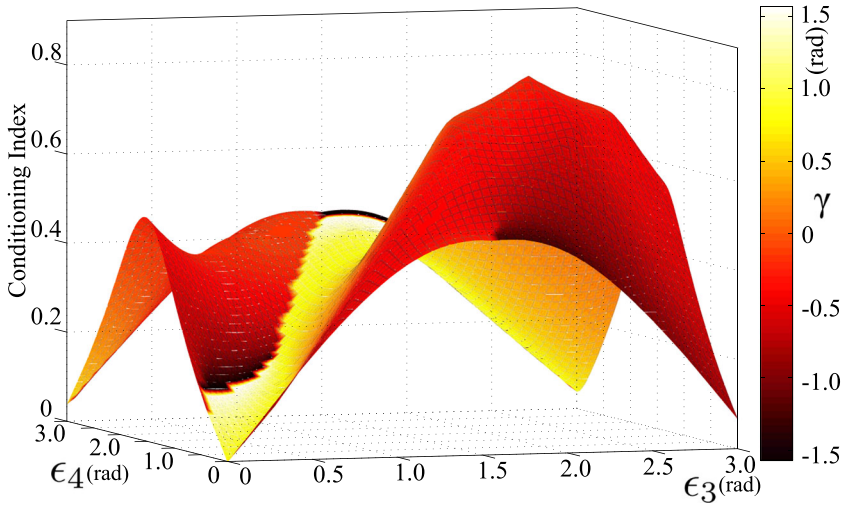

FIGURE 4 CI as a function of ϵ_3, ϵ_4 and γ for the best $v = -0.35$

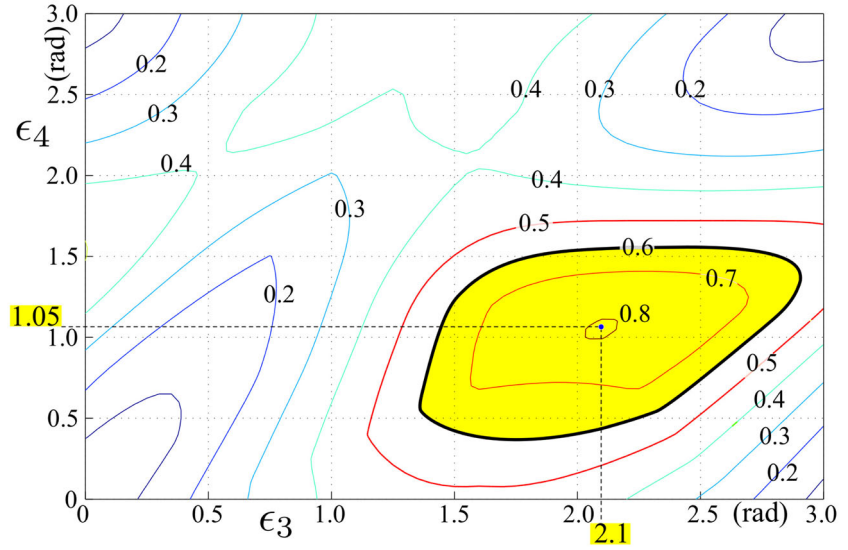

FIGURE 5 Contour curves for CI. The highlighted region provides CI > 0.6

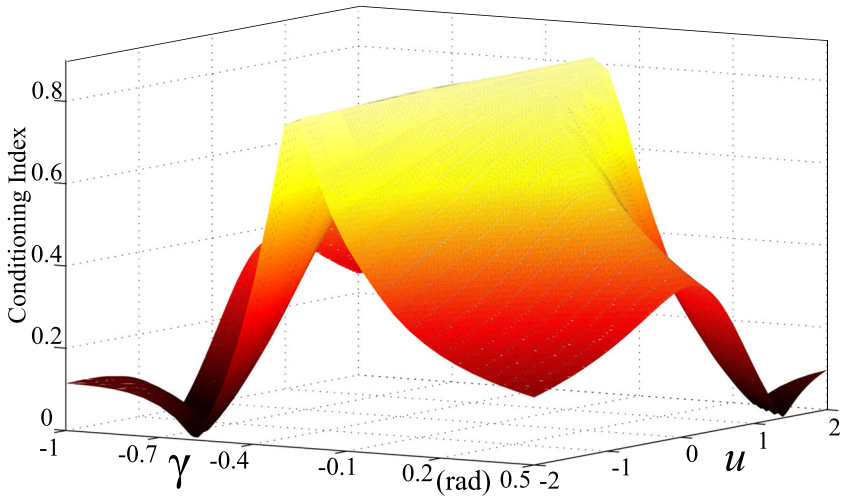

FIGURE 6 CI as a function of u and γ

support line r_2 should be perpendicular to r_1 when $u = 0.5$. By this way, keeping $u = 0.5$ and varying w and γ we have the CI shown in Figure 7.

Summarizing, CI reaches the maximum value for a triangular platform with $u = 0.5$, $w = 1$, $v = -0.35$, $\epsilon_3 = 2.1$ rad, $\epsilon_4 = 1.05$ rad, and $\gamma = -0.27$ rad. Thus ${}^{p}\mathbf{A}_3$ should be aligned with ${}^{p}\mathbf{A}_2$ and ${}^{p}\mathbf{A}_4$ for a maximum CI, in other words, the best geometry of the platform is an isosceles triangle shown in Figure 8.

5.2 | Workspace analysis

The CI optimization presented in Section 5.1 yielded the moving platform design, now allowing a performance analysis of the TetraFLEX's workspace.

Considering the designed moving platform, Figure 9 shows the 3D model of the PRRR + 3PRRS TetraFLEX with $l_{2i} = l_{3i} = 1.5$ u.l., and the triangular base platform with length side = 3.0 u.l., in the directions of $\mathbf{n}_2$ and $\mathbf{n}_4$.

Using the coordinates of $\mathbf{A}_1$ as tool's reference, the shape of the workspace depends on the angle γ and the resultant coordinates of A_j, $j = 2, 3, 4$. Such workspace is obtained by intersection of four right circular cylindrical shells due to the four P RRR-3P RRS legs (see Figure 1a). Each cylindrical shell, $i = 1, 2, 3, 4$, has the axis parallel to the $\mathbf{n}_i$ axis and passing through the point $\mathbf{H}_i$ computed as

$$\mathbf{H}_i = (\mathbf{O}_i - \mathbf{A}_i) - ((\mathbf{O}_i - \mathbf{A}_i) \cdot \mathbf{n}_i)\mathbf{n}_i \tag{29}$$

and inner outer radii equal do $l_{2i} - l_{3i}$ (for $l_{2i} > l_{3i}$) and $l_{2i} + l_{3i}$, respectively.

Figure 10a shows the 3D-diagram of the workspace for $l_{2i} = l_{3i} = 1.5$ u.l., $\gamma = -0.27$ rad and ${}^{p}\mathbf{A}_i$ as presented in Section 5.1.

It is interesting to note that the shape of the workspace has symmetry with respect to the $x_1 y_1$-plane (in $z_1 = 0$) and that the correspondent CI = 0.809 is the same for any point once $\gamma = -0.27$ rad is the unique variable in the $\mathbf{M}$ matrix (see Equation 24).

Complementary, the useful workspace is a regular geometric object located in the region of the workspace that satisfies some kinetostatics properties (Di Gregorio & Simas, 2016). Inspecting the

FIGURE 7 CI as a function of w and γ

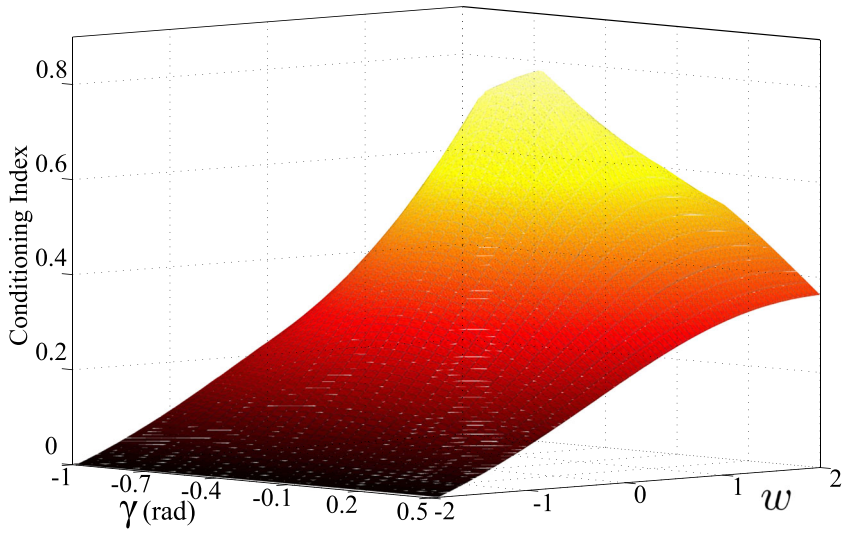

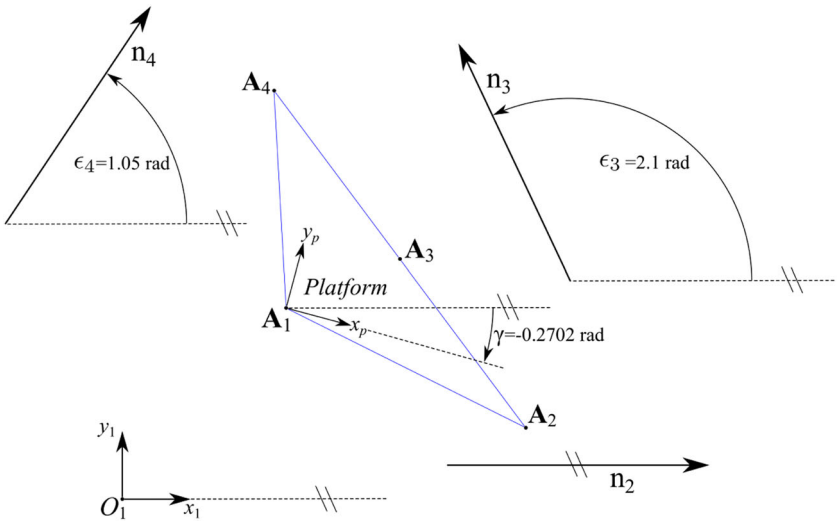

FIGURE 8 Optimal platform for TetraFLEX that provides the highest CI, i.e., CI = 0.809

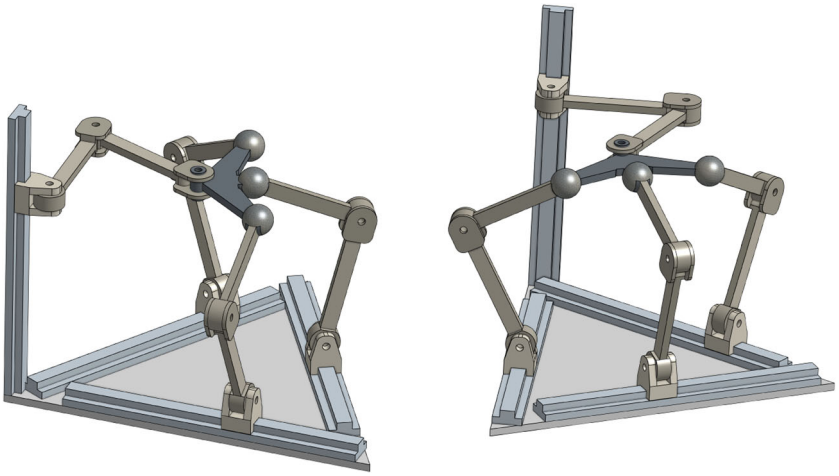

FIGURE 9 CAD model of the PRRR + 3PRRS TetraFLEX assembled according to the second solution of the FPA for the assigned active-joint positions (here, the angle γ does not correspond to the one ($\gamma = -0.27$ rad) that maximizes the CI)

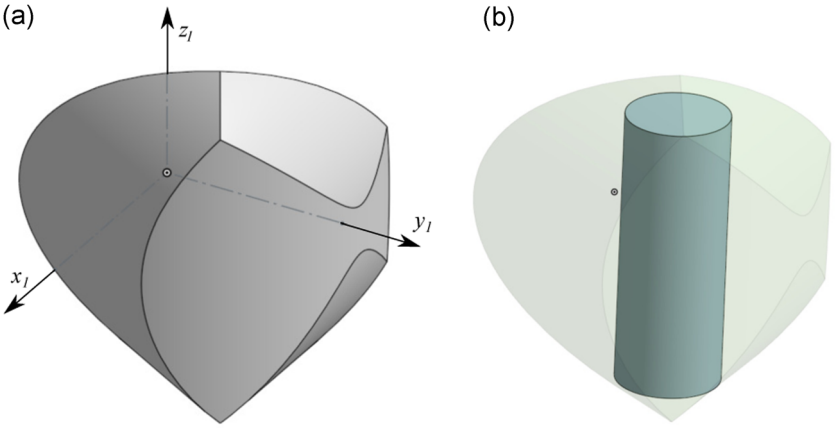

FIGURE 10 (a) Workspace volume of the PRRR + 3PRRS TetraFLEX and (b) chosen useful workspace

workspace the chosen useful workspace is equal to the regular cylinder, with axis parallel to z_1-axis, and delimited up and down by the planes parallel to $x_1 y_1$-plane for $z_1 = 2$ and $z_1 = -2$, respectively, defining the top and down surfaces. The base belonging to the cylinder is computed by maximal circle defined by three points on the resultant top and/or down surface. Figure 10b shows the corresponding useful workspace for the workspace.

Changing γ in the range $[-1, 0.5]$ rad, Figure 11 presents the correspondent computed volume of the cylindrical useful workspace as a function of γ.

5.3 | Inaccuracy due to base installation

Inaccuracies can happen when installing the base platform of TetraFLEX due mainly to the possible self-alignment variations, that implies in CI variations and consequently interfere with its performance, that is, due to the direction of the $\mathbf{n}_3$ and $\mathbf{n}_4$ vectors considering $\mathbf{n}_1$ and $\mathbf{n}_2$ vectors as reference vectors as discussed in previous sections.

Selecting the optimal triangular moving platform discussed in Figure 8, that is, setting $u = 0.5$, $w = 1$ $v = -0.35$, $\epsilon_3 = 2.1$ rad, $\epsilon_4 = 1.05$ rad, and $-1 \leq \gamma \leq 0.5$ rad, Figure 12 presents the maximal range of CI as a function of the inaccuracies around 1%, 5%, and 10% of the nominal values of ϵ_3 and ϵ_4. In other words the direction of vectors $\mathbf{n}_3$ and $\mathbf{n}_4$ were varied randomly by the desired percentage extracting the minimal maximal CI for each γ value.

Figure 12 shows the CI's range of variation, as a function of the geometry of the base for 10% of inaccuracy in *blue*, 5% results in *green*, and 1% in the *red*.

Choosing CI = 0.6 as the minimum performance limit, it is observed in Figure 12 that the available range of γ ($\Delta\gamma$) that guarantees such performance index, decreases as the percentage of imprecision of ϵ_3 and ϵ_4 increases. This analysis shows that it is necessary to control the accuracy of the base platform installation to guarantee a good range of platform orientation with good performance indices.

6 | DISCUSSION

The simple kinematics of TetraFLEX PMs makes it possible to conceive fast and easy calibration procedures. Indeed, the base geometric constants that appear in the above-reported kinematic analyses are n_{jx}, n_{jy}, n_{jz}, and $(\mathbf{O}_j \cdot \mathbf{n}_j)$, for $j = 2, 3, 4$. It is worth noting that the geometric constants of the platform refer to coordinates of points that belong to the same rigid body, which do not need to be redetermined when the machine is installed in a different place.

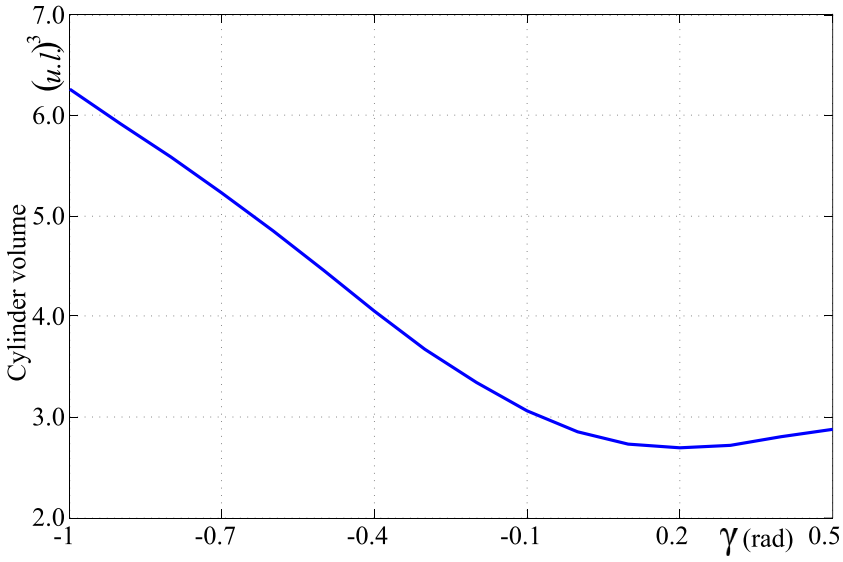

FIGURE 11 Volume of cylindrical useful workspace as a function of the angley

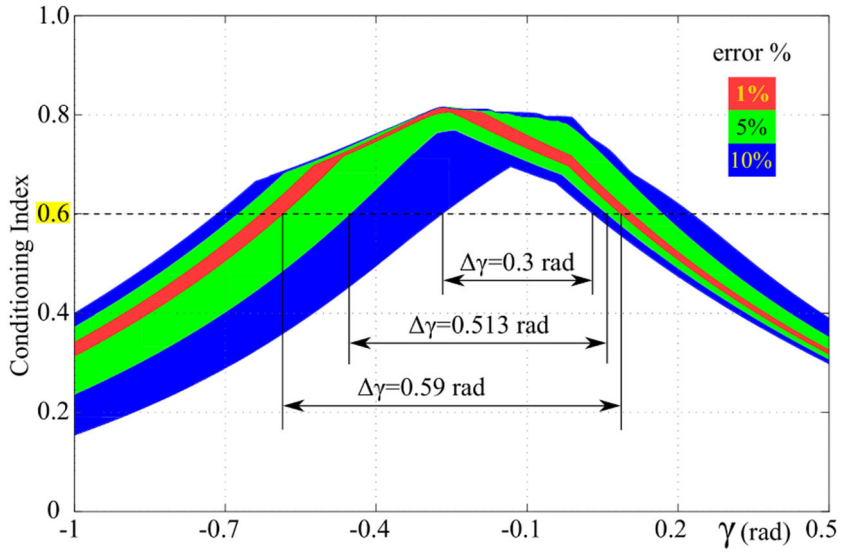

FIGURE 12 Sensitivity of the CI for the inaccuracies of 1% (red), 5% (green), and 10% (blue) due to the base installation

These constants are the only ones that a calibration procedure must determine when the TetraFLEX PM is installed in a new place. Such a procedure could be organized as follows:

- both the tuples **p** and **q** are measured for four different configurations of the TetraFLEX PM, and Equations (4) are written four times, once for each configuration;
- for each value of the j index greater than 1, the four corresponding equations are extracted from the ones written in the previous step;
- for each value of the j index greater than 1, the system of four equations, isolated in the previous step, which is linear in the four calibration unknowns n_{jx}, n_{jy}, n_{jz}, and $(\mathbf{O}_j \cdot \mathbf{n}_j)$, is solved.

As an alternative, a better calibration procedure, which takes into account the presence of measurement errors, consists in measuring **p** and **q** for more than four different configurations, and, then, in using more than four equations to compute the best estimate of n_{jx}, n_{jy}, n_{jz}, and $(\mathbf{O}_j \cdot \mathbf{n}_j)$ with the least squares method (Rencher & Christensen, 2012). Having an easy-to-implement calibration procedure is relevant in field robotics applications where the calibration procedure must be frequently repeated.

An other issue that deserves to be discussed is "How many types of TetraFLEX PMs can be identified?". The analysis that brings to identify all the possible mechanism topologies that satisfy assigned requirements is named type synthesis. There are several approaches for type synthesis. Evolutionary morphology (Gogu, 2008) virtual chain (Kong & Gosselin, 2007), displacements groups (Hervé, 1994), graphs and screw theory (Tsai, 1999) are the most known. Below, the approach proposed by Tsai (1999) is used.

The number of PM types that enter in the above-introduced generic topology P XYZ-3P QVWU depends on how many XYZ and QVW kinematic chains can be conceived. The XYZ chain is, by definition, a 3-DOF planar kinematic chain constituted by three

single-DOF pairs; as a consequence, if only P and R pairs are considered, there are only seven types of these chains: RRR, RPR, RRP, RPP, PRR, PPR, and PRP, where all the R-pairs (P-pairs) have their axes (their sliding directions) perpendicular (parallel) to the motion plane of the XYZ chain. It is worth reminding that, in a 3-DOF serial planar chain, no more than 2 P-pairs can be included. The QVW chain, by definition, constrains the center of the ending U-joint to move on a plane without limiting the platform orientation. If only P and R pairs are considered, the free motion of a point on a plane can be obtained by four 2-DOF planar chains: RR, PR, RP, and PP, where all the R-pairs (P-pairs) have their axes (their sliding directions) perpendicular (parallel) to the plane the point moves on. Then, the addition to any of these four 2-DOF chains of a third R-pair, as W pair, so disposed that it forms an S-pair with the ending U-joint (i.e., with the axis passing through the U-joint center and lying on the plane this center moves on) yields four kinematic chains that satisfy all the motion constraints imposed to the QVW chain. Such chains, when combined with the ending U-joint, give the following four QVWU kinematic chains: RRS, PRS, RPS, and PPS, where all the R-pairs (P-pairs) have their axes (their sliding directions) perpendicular (parallel) to the plane the S-pair center moves on. Particular cases of these four QVWU chains can be obtained by combining a passive RP or PR sub-chain into a C pair when the axis of the R-pair is parallel to the sliding direction of the P-pair (see Figure 1b). In short, these simple considerations bring to identify 28 (= 7 × 4) different types of TetraFLEX PMs for which all the above-deduced results hold unchanged. This number can be further increased if the fact that nothing changes when the three PQVWU limbs have different topologies is considered and, over P and R pairs, other types of single-DOF pairs (e.g., π joints) are taken into account.

Eventually, it is worth stressing that the actuated P-pairs located on the base can be manufactured in many different ways according to the particular context the TetraFLEX PM has to work. For instance, in field robotics applications, they could be obtained through a trolley that moves on a rail track and has bilateral contacts with the rail; indeed, such a layout allows the fixation of the rails on different terrains and with different arrangements, which is a sought-after feature when a crane has to be mounted in a building site. Differently, in industrial applications, they could be obtained through precise linear guides embedded in a unique link that constitutes a fixed-geometry base. Also, a full rotation of a possible gripper mounted on the platform can be obtained through suitable rotation amplifiers like the simple one described in Simas and Di Gregorio (2017, 2019), which uses a toothed-belt transmission. Therefore, TetraFLEX PMs lend themselves to a wide variety of applications.

Regarding the simulations, as it can be seen in Section 5.1, TetraFLEX has good performance in several configurations of the base and the platform. This characteristics is due to the self-aligning and it is relevant to install TetraFLEX in an unstructured environment of field robotics. Also, once TetraFLEX is installed, the angles ϵ_j, $j = 2, 3, 4$ are defined and a correct variation of γ must to be set to improve the performance and to avoid singularities (see details in Figures 4, 5, and 12). Such results also shows TetraFLEX robot is robust enough to keep out of singular postures even with inaccuracies in the axis of sliding joints in the base.

Regarding applications, TetraFLEX can be used in unstructured environments of field robotics for complex tasks, for example, building, mining, rescue, as well as for pick and place in industrial applications. As discussed in the text, the self-aligning property makes TetraFLEX easy to mount and calibrate because once it has the $\mathbf{n}_j$, $j = 1, 2, 3, 4$ linearly independent it works according to the model developed in this paper.

Another advantage of TetraFLEX that is relevant for applications in remote environments of field robotics is its prismatic actuation with sliding direction fixed to the base. Indeed, such feature makes the structure of the limbs conceivable as foldable and deployable trusses (e.g., like a building crane) that, when folded, are compact and easy to transport and, when deployed on site, can be assembled and calibrated to operate. Foldable/deployable machines, over in building sites, are of particular interest in aerospace missions.

7 | CONCLUSION

A new family of 3T1R PMs, named TetraFLEX, has been identified. The PMs of this family have the same finite and instantaneous kinematics. In particular, they share the same closure equations and instantaneous input/output relationship, which made it possible to present a unique kinematics analysis and singularity determination for all of them.

These analyses proved that their position analysis has reachable solution in closed form and that they have no constraint singularity with only two type-II singularities easy to find and avoid. Also, their architecture singularities have been all identified and how to exclude them during design has been explained.

The simplicity of their kinematics has allowed to present simple calibration procedures, which is a sought-after feature in field robotics. Moreover, the design criteria that optimize their kinematic performances/accuracies have been proposed and applied to a case study. The case study proved that TetraFLEX PMs are self-aligning PMs, that is, they compensate possible installation inaccuracies for a wide range of base-geometry perturbations, which is another appealing feature in field robotics.

The design of the TetraFLEX PMs family, with all its properties, leads us to several future developments, including the development of prototypes, experiments for performance evaluation in the fields of robotics with unstructured environments such as civilian construction, mining, welding structures (ship hulls, for example) and special applications, make the most of the self-alignment property.

In a complementary way, advancing the TetraFLEX family in dynamic models and the proposition of control strategies in physical prototypes allows new application propositions to turn it into a future product.

ACKNOWLEDGMENTS

This study has been supported by UNIFE—University of Ferrara—grant no. FAR2020—Italy and by CNPq—Conselho Nacional de

Desenvolvimento Científico e Tecnológico (National Council for Scientific and Technological Development)—Project no 309241/2017-0—Brazil. Open Access Funding provided by Universita degli Studi di Ferrara within the CRUI-CARE Agreement.

REFERENCES

Agrawal, S. (1991) Workspace boundaries of in-parallel manipulator systems. In: *Fifth International Conference on Advanced Robotics 'Robots in Unstructured Environments*, Vol. *2*, Pisa, Italy: IEEE. pp. 1147–1152. https://doi.org/10.1109/ICAR.1991.240401

Amine, S., Nurahmi, L., Wenger, P. & Caro, S. (2013) Conceptual design of Schoenflies motion generators based on the wrench graph. In: *ASME 2013 International Design Engineering Technical Conferences and Computers and Information in Engineering Conference*. American Society of Mechanical Engineers Digital Collection.

Arian, A., Isaksson, M. & Gosselin, C. (2020) Kinematic and dynamic analysis of a novel parallel kinematic Schönflies motion generator. *Mechanism and Machine Theory*, *147*, 103629.

Briot, S. & Bonev, I.A. (2009) Pantopteron: a new fully decoupled 3DOF translational parallel robot for pick-and-place applications. *Journal of Mechanisms and Robotics*, *1*(2), 170f92-33f3-4834-bdf9-9cc0a9c88a40">–9.

Briot, S. & Bonev, I.A. (2010) Pantopteron-4: a new 3t1r decoupled parallel manipulator for pick-and-place applications. *Mechanism and Machine Theory*, *45*(5), 707–721.

Carricato, M. (2005) Fully isotropic four-degrees-of-freedom parallel mechanisms for Schoenflies motion. *The International Journal of Robotics Research*, *24*(5), 397–414.

Clavel, R. (1990) *Device for the movement and positioning of an element in space*, U.S. Patent No. US4976582, December 11.

Davidson, J.K. & Hunt, K.H. (2004) *Robots and screw theory: Applications of kinematics and statics to robotics*. Oxford: Oxford University Press.

Di Gregorio, R. (2017) A novel single-loop decoupled Schoenflies-motion generator: Concept and kinematics analysis. In: *International Conference on Robotics in Alpe-Adria Danube Region*. Springer, pp. 11–18.

Di Gregorio, R. (2020) A review of the literature on the lower-mobility parallel manipulators of 3-UPU or 3-URU type. *Robotics*, *9*(1), 5.

Di Gregorio, R., Cattai, M. & Simas, H. (2018) Performance-based design of the CRS-RRC Schoenflies-motion generator. *Robotics*, *7*(3), 55.

Di Gregorio, R. & Simas, H. (2016) Dimensional synthesis of the single-loop translational parallel manipulator PRR-PRPU. Meccanica.

Gallardo-Alvarado, J., García-Murillo, M.A., Islam, M.N. & Abedinnasab, M.H. (2017) Kinematics of the 4-RUU parallel manipulator generator of the Schönflies motion by means of screw theory. *Journal of Mechanical Science and Technology*, *31*(10), 4925–4932.

Gogu, G. (2008) *Structural synthesis of parallel robots*. Part of the solid mechanics and its applications book series (SMIA, volume 149). Dordrecht: Springer.

Gosselin, C. (2009) Compact dynamic models for the tripteron and quadrupteron parallel manipulators. *Proceedings of the Institution of Mechanical Engineers, Part I: Journal of Systems and Control Engineering*, *223*(1), 1–12.

Gosselin, C. & Angeles, J. (1991) A global performance index for the kinematic optimization of robotic manipulators. *Journal of Mechanical Design (1990)*, *113*(3), 220–226.

Gosselin, C.M. & Angeles, J. (1990) Singularity analysis of closed-loop kinematic chains. *IEEE Transactions on Robotics and Automation*, *6*(3), 281–290.

Gosselin, C.M., Masouleh, M.T., Duchaine, V., Richard, P.-L., Foucault, S. & Kong, X. (2007) Parallel mechanisms of the multipteron family: kinematic architectures and benchmarking. In: *Proceedings 2007 IEEE International Conference on Robotics and Automation*. IEEE, pp. 555–560.

Hervé, J.M. (1994) The mathematical group structure of the set of displacements. *Mechanism and Machine Theory*, *29*(1), 73–81.

Hervé, J.M. (1999) The lie group of rigid body displacements, a fundamental tool for mechanism design. *Mechanism and Machine Theory*, *34*, 719–730.

Kong, X. & Gosselin, C. (2007) *Type synthesis of parallel mechanisms*. New York: Springer.

Kong, X. & Gosselin, C.M. (2004) Type synthesis of 3t1r 4-DOF parallel manipulators based on screw theory. *IEEE Transactions on Robotics and Automation*, *20*(2), 181–190.

Krut, S., Company, O., Benoit, M., Ota, H. & Pierrot, F. (2003) I4: a new parallel mechanism for scara motions. In: *Procs. of IEEE ICRA'03: Int. Conf. on Robotics and Automation*. IEEE, pp. 1875–1880.

Krut, S., Nabat, V., Company, O. & Pierrot, F. (2004) A high speed robot for Scara motions. In: *Procs. of IEEE ICRA'04: Int. Conf. on Robotics and Automation*. IEEE, pp. 4109–4115.

Lee, C.-C. & Hervé, J.M. (2009a) On some applications of primitive Schönflies-motion generators. *Mechanism and Machine Theory*, *44*, 2153–2163.

Lee, C.-C. & Hervé, J.M. (2009b) Type synthesis of primitive Schoenflies-motion generators. *Mechanism and Machine Theory*, *44*, 1980–1997.

Lee, C.-C. & Hervé, J.M. (2009c) Uncoupled actuation of overconstrained 3t-1r hybrid parallel manipulators. *Robotica*, *27*, 103–117.

Lee, C.-C. & Hervé, J. M. (2011) Isoconstrained parallel generators of Schoenflies motion. ASME Journal of Mechanisms and Robotics, 3(May 2011), 021006 (10pages).

Lee, P.-C. & Lee, J.-J. (2012) Singularity and workspace analysis of three isoconstrained parallel manipulators with Schoenflies motion. *Frontiers of Mechanical Engineering*, *7*(2), 163–187.

Lee, P.-C. & Lee, J.-J. (2016) On the kinematics of a new parallel mechanism with Schoenflies motion. *Robotica*, *34*(9), 2056–2070.

Ma, O. & Angeles, J. (1991) Architecture singularities of platform manipulators. In: *Proceedings. 1991 IEEE International Conference on Robotics and Automation*, Vol. 2. pp. 1542–1547.

Makino, H. (1982) *Assembly robot*. U.S. Patent No. US4341502, July 27.

Maletz, E.R., Meneghini, L., Grando, M.T., Martins, D., Simoni, R. & Simas, H. (2019) Triflex u-kinematic and error analysis of a self-aligned translational parallel manipulator prru. In: *IFToMM World Congress on Mechanism and Machine Science*. Springer, pp. 2641–2650.

Merlet, J.-P. (2006) *Parallel robots*. Part of the solid mechanics and its applications book series (SMIA, volume 128). Dordrecht: Springer.

Pierrot, F. & Company, O. (1999) H4: a new family of 4-DOF parallel robots. In: *Proceedings of AIM'99: IEEE/ASME International Conference on Advanced Intelligent Mechatronics*. IEEE/ASME, pp. 508–513.

Pierrot, F., Company, O., Krut, S. & Nabat, V. (2006) Four-DOF PKM with articulated travelling-plate. In: *Procs. of PKS'06: Parallel Kinematics Seminar*. pp. 25–26. Available at: https://hal-lirmm.ccsd.cnrs.fr/lirmm-00105558. [Accessed 24th April 2021].

Pierrot, F., Nabat, V., Company, O., Krut, S. & Poignet, P. (2009) Optimal design of a 4-dof parallel manipulator: From academia to industry. *IEEE Transactions on Robotics*, *25*(2), 213–224.

Rat, N., Neagoe, M. & Gogu, G. (2010) Theoretical and experimental research on the dynamics of a 4DOF isoglide 4-t3r1 parallel robot. In: *SYROM 2009*. Springer, pp. 387–396.

Rencher, A. C. & Christensen, W. F. (2012) *Methods of multivariate analysis*. Hoboken, NJ: John Wiley & Sons, Inc.

Simas, H. & Di Gregorio, R. (2017) Kinematics of a particular 3t1r parallel manipulator of type 2PRPU. In: *ASME 2017 International Design Engineering Technical Conferences and Computers and Information in Engineering Conference*. American Society of Mechanical Engineers Digital Collection.

Simas, H. & Di Gregorio, R. (2019) Position analysis, singularity loci and workspace of a novel 2PRPU Schoenflies-motion generator. *Robotica*, *37*(1), 141–160.

Simas, H., Simoni, R. & Martins, D. (2017) Triflex II: design and analysis of a self-aligning parallel mechanism with asymmetrical kinematic structure. *Meccanica*, *52*(11–12), 2991–3002.

Simoni, R., Simas, H. & Martins, D. (2014) Triflex: Design and prototyping of a 3-DOF variable-configuration parallel manipulator with self-aligning. *International Journal of Mechanical Engineering and Automation*, *1*(2), 77–82.

Simoni, R., Simas, H. & Martins, D. (2015) Triflex: variable-configuration parallel manipulators with self-aligning. *Journal of the Brazilian Society of Mechanical Sciences and Engineering*, *37*(4), 1129–1138.

Tsai, L.-W. (1999) *Robot analysis: the Mechanics of serial and parallel manipulators*. New York: John Wiley & Sons.

Tu, Y., Chen, Q., Ye, W. & Li, Q. (2018) Kinematics, singularity, and optimal design of a novel 3t1r parallel manipulator with full rotational capability. *Journal of Mechanical Science and Technology*, *32*(6): 2877–2887.

Zlatanov, D., Bonev, I. & Gosselin, C. (2002). Constraint singularities of parallel mechanisms. In: *Proceedings 2002 IEEE International Conference on Robotics and Automation (Cat. No.02CH37292)*, Vol. *1*. pp. 496–502.

How to cite this article: Simas, H., Di Gregorio, R. & Simoni, R. (2022). TetraFLEX: Design and kinematic analysis of a novel self-aligning family of 3T1R parallel manipulators. *Journal of Field Robotics*, 39, 617–630.
https://doi.org/10.1002/rob.22067